# Supporting Information

## Selective sensing of 2,4,6-trinitrophenol (TNP) in aqueous media with "aggregation-induced emission enhancement" (AIEE)-active iridium(III) complexes

Weilong Che,[a] Guangfu Li,[a] Xingman Liu,[a] Kuizhan Shao,[a] Dongxia Zhu,*[a] Zhongmin Su*[a] and Martin R. Bryce*[b]

[a] Key Laboratory of Nanobiosensing and Nanobioanalysis at Universities of Jilin Province, Department of Chemistry, Northeast Normal University, 5268 Renmin Street, Changchun, Jilin Province 130024, P.R. China E-mail: zhudx047@nenu.edu.cn, zmsu@nenu.edu.cn

[b] Department of Chemistry, Durham University, Durham, DH1 3LE, UK
E-mail: m.r.bryce@durham.ac.uk

## Table of Contents



### 1. Experimental - general information

Materials obtained from commercial suppliers were used without further purification unless otherwise stated. All glassware, syringes, magnetic stirring bars, and needles were thoroughly dried in a convection oven. Reactions were monitored using thin layer chromatography (TLC).

Commercial TLC plates were used and the spots were visualised under UV light at 254 and 365 nm. $^1$H NMR spectra were recorded at 25 ºC on a Varian 500 MHz spectrometer. The chemical shifts (δ) are given in parts per million relative to internal standard TMS. The $^1$H NMR spectra were referenced internally to the residual proton resonance in DMSO-$d_6$ ($\delta$ 2.49 ppm). The molecular weights of the complexes were obtained by using matrix-assisted laser desorption-ionization time-of-flight (MALDI-TOF) mass spectrometry. Elemental analysis was obtained using a Flash EA1112 analyser. UV-vis absorption spectra were recorded on a Shimadzu UV-3100 spectrophotometer. Photoluminescence spectra were collected on a Shimadzu RF-5301pc spectrophotometer and a Maya 2000Pro optical fiber spectrophotometer. PL efficiencies were measured with an integrating sphere (C-701, Labsphere Inc.) with a 365 nm Ocean Optics LLS-LED as the excitation source, and the laser was introduced into the sphere through the optical fiber.

## 2. Complexes 1-4 - synthesis and characterization

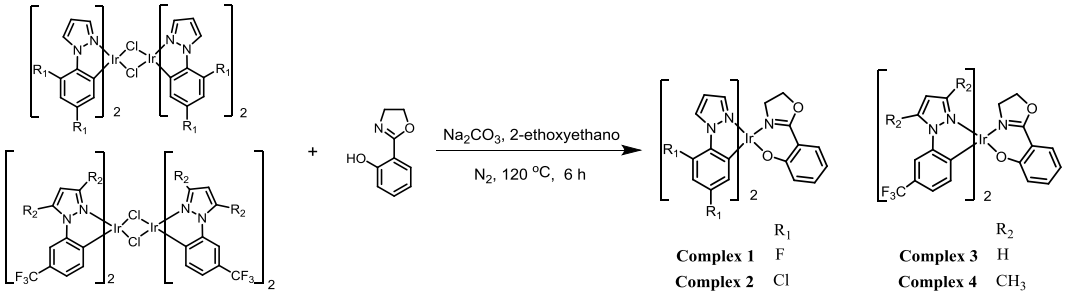


**Scheme S1** Synthetic route to complexes **1-4**.

**Synthesis of [(1-(2,4-difluorophenyl)-1H-pyrazole)$_2$Ir(oz)] (complex 1)**

A procedure in the literature was applied for the synthesis of Hoz.[1] The complex [(1-(2,4-difluorophenyl)-1H-pyrazole)$_2$Ir(μ-Cl)]$_2$ was synthesized by the standard procedure.[2] A mixture of [(1-(2,4-difluorophenyl)-1H-pyrazole)$_2$Ir(μ-Cl)]$_2$ (0.375 g, 0.330 mmol), $Na_2CO_3$ (0.349 g, 3.20 mmol), and Hoz (0.114 g, 0.70 mmol) dissolved in 2-ethoxyethanol (30 mL) was stirred under an $N_2$ atmosphere at 130 ºC for 6 h. EtOAc (150 mL) was added after the solution was cooled to RT and washed with water (100 mL) to remove 2-ethoxyethanol. The precipitate was collected by filtration and washed with ethanol (20 mL), followed by diethyl ether (10 mL). Silica gel column purification with n-hexane: EtOAc (5:1 v/v) as eluent gave complex **1** as a green powder (0.329 g, 70% yield). $^1$H NMR (DMSO-$d_6$, 500 MHz, δ [ppm]) δ 8.58 (d, $J$ = 5 Hz, 2H), 8.03 (d, $J$ = 3 Hz, 1H), 7.53 (d, $J$ = 5 Hz, 1H), 7.50 (d, $J$ = 2 Hz, 1H), 7.10 (t, $J$ = 6 Hz, 1H) 6.84-6.89 (m, 4H), 6.51 (d, $J$ = 8 Hz, 1H), 6.33 (t, $J$ = 10 Hz, 1H), 5.63 (d, $J$ = 5 Hz, 1H), 5.51 (d, $J$ = 7.5 Hz, 1H), 4.44-4.49 (m, 1H), 4.28-4.33 (m, 1H), 3.71-3.76 (m, 1H), 2.98-3.03 (m, 1H). MS: m/z = 713.10 ($M^+$). Anal. calcd for $C_{27}H_{18}F_4IrN_5O_2$: C 45.50, H 2.55, N 9.83; found: C 45.62, H 2.73, N 9.64. Crystals for X-ray analysis were obtained by slow evaporation of a dichloromethane-methanol solution of the complex.

**Synthesis of [(1-(2,4-dichlorophenyl)-1H-pyrazole)$_2$Ir(oz)] (complex 2)**

The synthesis of complex **2** was similar to that of complex **1** except that the cyclometalated ligand used for **2** was 1-(2,4-dichlorophenyl)-1H-pyrazole. Complex **2** was obtained as a yellowish-green solid (0.374 g, 73% yield). $^1$H NMR (DMSO-$d_6$, 500 MHz, δ [ppm]) δ 9.21 (t,

*J* = 7.5 Hz, 2H), 8.11 (d, *J* = 2. Hz, 1H), 7.58 (d, *J* = 2. Hz, 1H), 7.52 (d, *J* = 5 Hz, 1H), 7.17 (d, *J* = 2.5 Hz, 1H), 7.14 (d, *J* = 2 Hz, 1H), 7.09 (t, *J* = 5 Hz, 1H), 6.92 (s, 2H), 6.50 (d, *J* = 7 Hz, 1H), 6.33 (t, *J* = 6 Hz, 1H), 5.95 (d, *J* = 2 Hz, 1H), 5.81 (d, *J* = 2.5 Hz, 1H), 4.43-4.48 (m, 1H), 4.28-4.33 (m, 1H), 3.67-3.72 (m, 1H), 2.93-2.98 (m, 1H). MS: m/z = 776.98 ($M^+$). Anal. calcd for $C_{27}H_{18}Cl_4IrN_5O_2$: C 41.66, H 2.33, N 9.00; found: C 41.83, H 2.27, N 9.04.

**Synthesis of [(1-(3-(trifluoromethyl)phenyl)-1H-pyrazole)$_2$Ir(oz)] (complex 3)**

The synthesis of complex **3** was similar to that of complex **1** except that the cyclometalated ligand used for **3** was 1-(3-(trifluoromethyl)phenyl)-1H-pyrazole. Complex **3** was obtained as a green solid (0.338 g, 66% yield). $^1$H NMR (DMSO-$d_6$, 500 MHz, δ [ppm]) δ 9.04 (t, *J* = 5 Hz, 2H), 8.00 (d, *J* = 2.5 Hz, 1H), 7.97 (s, 2H), 7.52 (d, *J* = 7.5 Hz, 1H), 7.48 (d, *J* = 3 Hz, 1H), 7.07 (t, *J* = 7.5 Hz, 1H), 6.94 (t, *J* = 7.5 Hz, 2H), 6.84-6.86 (m, 2H), 6.47 (d, *J* = 10 Hz, 1H), 6.36 (d, *J* = 6.5 Hz, 1H), 6.30 (t, *J* = 6 Hz, 1H), 6.25 (d, *J* = 7 Hz, 1H), 4.40-4.45 (m, 1H), 4.25-4.29 (m, 1H), 3.67-3.70 (m, 1H), 2.92-2.95 (m, 1H). MS: m/z = 777.12 ($M^+$). Anal. calcd for $C_{29}H_{20}F_6IrN_5O_2$: C 44.84, H 2.60, N 9.02; found: C 44.96, H 2.52, N 6.21.

**Synthesis of [(3,5-dimethyl-1-(3-(trifluoromethyl)phenyl)-1H-pyrazole)$_2$Ir(oz)] (complex 4)**

The synthesis of complex **4** was similar to that of complex **1** except that the cyclometalated ligand used for **4** was 3,5-dimethyl-1-(3-(trifluoromethyl)phenyl)-1H-pyrazole. Complex **4** was obtained as a yellowish-green solid (0.379 g, 69% yield). $^1$H NMR (DMSO-$d_6$, 500 MHz, δ [ppm]) δ 7.54 (t, *J* = 10 Hz, 3H), 7.03 (t, *J* = 6 Hz, 1H), 6.93 (d, *J* = 7.5 Hz, 2H), 6.48 (s, 1H), 6.43 (d, *J* = 7 Hz, 1H), 6.41 (s, 1H), 6.37 (d, *J* = 7 Hz, 1H), 6.32 (d, *J* = 6.5 Hz, 1H), 6.26 (t, *J* = 6 Hz, 1H), 4.26-4.30 (m, 1H), 4.21-4.25 (m, 1H), 3.41-3.45 (m, 1H), 2.91-2.95 (m, 1H), 2.89 (s, 3H), 2.87 (s, 3H), 2.27 (s, 3H), 2.21 (s, 3H). MS: m/z = 833.18 ($M^+$). Anal. calcd for $C_{33}H_{28}F_6IrN_5O_2$: C 47.59, H 3.39, N 8.41; found: C 47.71, H 3.32, N 8.33.

## 3. X-ray crystallographic data

The single crystals of complexes **1-4**, and complex **1**·**TNP**, were obtained by slow evaporation of the compounds dissolved on a dichloromethane-methanol (3:1 v/v) solution (for **1-4**) and a dichloromethane solution (for **1**·**TNP**). For crystal growth of **1**·**TNP**, **1** and **TNP** were mixed in a 1:1 molar ratio. Diffraction data were collected on a Bruker SMART Apex CCD diffractometer using k(Mo-K) radiation (k = 0.71073 Å). Cell refinement and data reduction were made by the SAINT program. The structures were determined using the SHELXTL/PC program. All non-hydrogen atoms were refined anisotropically, whereas hydrogen atoms were placed at the calculated positions and included in the final stage of refinements with fixed parameters. Fig. 3, Fig. S6-S8 and Fig. 7 show Oak Ridge thermal ellipsoid plot (ORTEP) drawings of complexes **1-4** and complex **1**·**TNP**, and crystallographic data for them have been deposited with the Cambridge Crystallographic Data Centre with CCDC deposition number 1573144, 1573145, 1573146, 1573147 and 1573148. These data can be obtained free of charge from The Cambridge Crystallographic Data Centre via www.ccdc.cam.ac.uk/data_request/cif.

**Table S1.** Crystal data and structure refinement for complex **1**.

| | Complex **1** |
|---|---|
| Empirical formula | $C_{27}H_{18}F_4IrN_5O_2$ |
| Formula weight | 720.66 |
| Temperature (K) | 293(2) |
| Crystal system | Tetragonal |
| Space group | I4(1)/a |
| a /Å | 27.885(6) |
| b /Å | 27.885 |
| c /Å | 12.931(3) |
| α /° | 90.000 |
| β /° | 90.000 |
| γ /° | 90.000 |
| V/Å$^3$ | 10055(3) |
| Z | 16 |
| $\rho_{calc}$ (g/cm$^3$) | 1.904 |
| μ/mm$^{-1}$ | 5.379 |
| $R_{int}$ | 0.0484 |
| Goodness-of-fit on $F^2$ | 1.107 |
| $R_1$[a], $wR_2$[b] [I>2σ(I)] | 0.0265, 0.0658 |
| $R_1$, $wR_2$ (all data) | 0.0370, 0.0796 |

[a] $R_1 = \Sigma||Fo| - |Fc||/\Sigma|Fo|$. [b] $wR_2 = \{ \Sigma[ w( Fo^2 - Fc^2)^2]/ \Sigma[w(Fo^2)^2]\}^{1/2}$

**Table S2.** Crystal data and structure refinement for complex **2**.

| | Complex **2** |
|---|---|
| Empirical formula | $C_{27}H_{18}Cl_4IrN_5O_2$ |
| Formula weight | 778.46 |
| Temperature (K) | 293(2) |
| Crystal system | Triclinic |
| Space group | P-1 |
| a /Å | 11.546(16) |
| b /Å | 13.292(19) |
| c /Å | 13.599(19) |
| α /° | 109.302(3) |
| β /° | 110.410(2) |
| γ /° | 103.766(3) |
| V/Å$^3$ | 1692.5(4) |
| Z | 2 |
| $\rho_{calc}$ (g/cm$^3$) | 1.528 |
| μ/mm$^{-1}$ | 4.289 |
| $R_{int}$ | 0.0416 |
| Goodness-of-fit on $F^2$ | 1.041 |
| $R_1$[a], $wR_2$[b] [I>2σ(I)] | 0.0735, 0.2119 |

| | |
|---|---|
| $R_1$, $wR_2$ (all data) | 0.1148, 0.2491 |

[a] $R_1 = \Sigma||Fo| - |Fc||/\Sigma|Fo|$. [b] $wR_2 = \{ \Sigma[ w( Fo^2 - Fc^2)^2]/ \Sigma[w(Fo^2)^2]\}^{1/2}$

**Table S3.** Crystal data and structure refinement for complex **3**.

| | Complex **3** |
|---|---|
| Empirical formula | $C_{30}H_{24}F_6IrN_5O_3$ |
| Formula weight | 808.74 |
| Temperature (K) | 293(2) |
| Crystal system | Monoclinic |
| Space group | P2(1)/n |
| a /Å | 13.872(16) |
| b /Å | 10.096(12) |
| c /Å | 22.338(3) |
| α /° | 90.000 |
| β /° | 105.767(2) |
| γ /° | 90.000 |
| V/Å$^3$ | 3010.8(6) |
| Z | 4 |
| $\rho_{calc}$ (g/cm$^3$) | 1.784 |
| μ/mm$^{-1}$ | 4.512 |
| $R_{int}$ | 0.0548 |
| Goodness-of-fit on $F^2$ | 0.939 |
| $R_1$[a], $wR_2$[b] [I>2σ(I)] | 0.0405, 0.0897 |
| $R_1$, $wR_2$ (all data) | 0.0734, 0.1010 |

[a] $R_1 = \Sigma||Fo| - |Fc||/\Sigma|Fo|$. [b] $wR_2 = \{ \Sigma[ w( Fo^2 - Fc^2)^2]/ \Sigma[w(Fo^2)^2]\}^{1/2}$

**Table S4.** Crystal data and structure refinement for complex **4**.

| | Complex **4** |
|---|---|
| Empirical formula | $C_{33}H_{28}F_6IrN_5O_2$ |
| Formula weight | 832.80 |
| Temperature (K) | 293(2) |
| Crystal system | Triclinic |
| Space group | P-1 |
| a /Å | 10.047(8) |
| b /Å | 11.116(8) |
| c /Å | 16.257(13) |
| α /° | 98.712(13) |
| β /° | 104.853(14) |
| γ /° | 98.326(14) |
| V/Å$^3$ | 1702.4(2) |
| Z | 2 |
| $\rho_{calc}$ (g/cm$^3$) | 1.625 |
| μ/mm$^{-1}$ | 3.991 |
| $R_{int}$ | 0.0227 |
| Goodness-of-fit on $F^2$ | 1.037 |

| | |
|---|---|
| $R_1$[a], $wR_2$[b] [I>2σ(I)] | 0.0689, 0.1896 |
| $R_1$, $wR_2$ (all data) | 0.0896, 0.2085 |

[a] $R_1 = \Sigma||Fo| - |Fc||/\Sigma|Fo|$. [b] $wR_2 = \{ \Sigma[ w( Fo^2 - Fc^2)^2]/ \Sigma[w(Fo^2)^2]\}^{1/2}$

**Table S5.** Crystal data and structure refinement for complex **1**·**TNP**.

| | Complex **1**·**TNP** |
|---|---|
| Empirical formula | $C_{33}H_{21}F_4IrN_8O_9$ |
| Formula weight | 941.78 |
| Temperature (K) | 293(2) |
| Crystal system | Monoclinic |
| Space group | P2(1)/n |
| a /Å | 17.161(3) |
| b /Å | 9.905(2) |
| c /Å | 23.645(5) |
| α /° | 90.000(3) |
| β /° | 104.930(3) |
| γ /° | 90.000(3) |
| V/Å$^3$ | 3883.6(13) |
| Z | 4 |
| $\rho_{calc}$ (g/cm$^3$) | 1.611 |
| μ/mm$^{-1}$ | 3.517 |
| $R_{int}$ | 0.0730 |
| Goodness-of-fit on $F^2$ | 1.219 |
| $R_1$[a], $wR_2$[b] [I>2σ(I)] | 0.0481, 0.1390 |
| $R_1$, $wR_2$ (all data) | 0.0743, 0.1606 |

[a] $R_1 = \Sigma||Fo| - |Fc||/\Sigma|Fo|$. [b] $wR_2 = \{ \Sigma[ w( Fo^2 - Fc^2)^2]/ \Sigma[w(Fo^2)^2]\}^{1/2}$

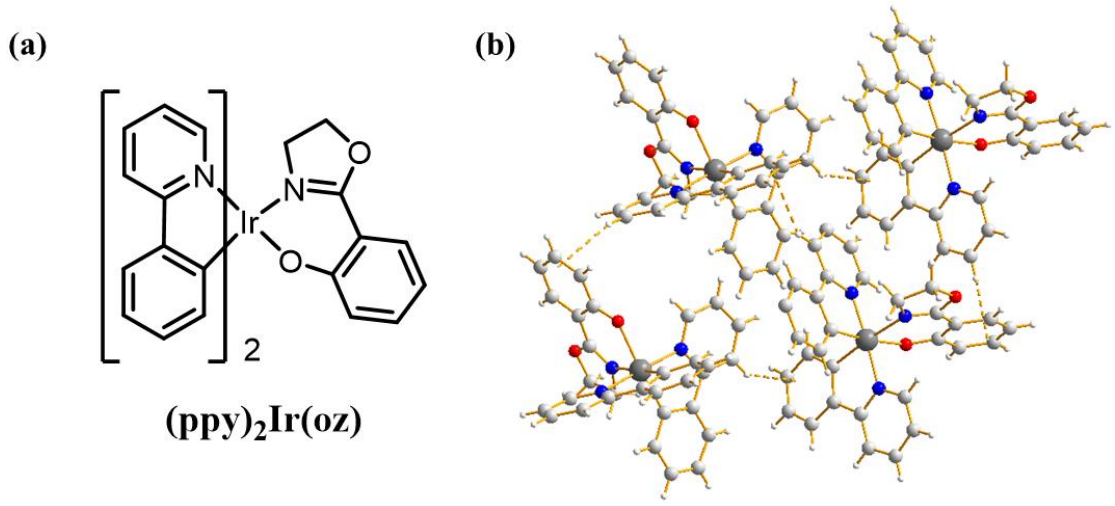


**Fig. S1** (a) Chemical structure of $(ppy)_2Ir(oz)$. (b) Molecular packing of $(ppy)_2Ir(oz)$ in the crystal. Data taken from K. Chao, et al, *J. Mater. Chem. C.*, 2013, **1**, 6800. CCDC number 835020.

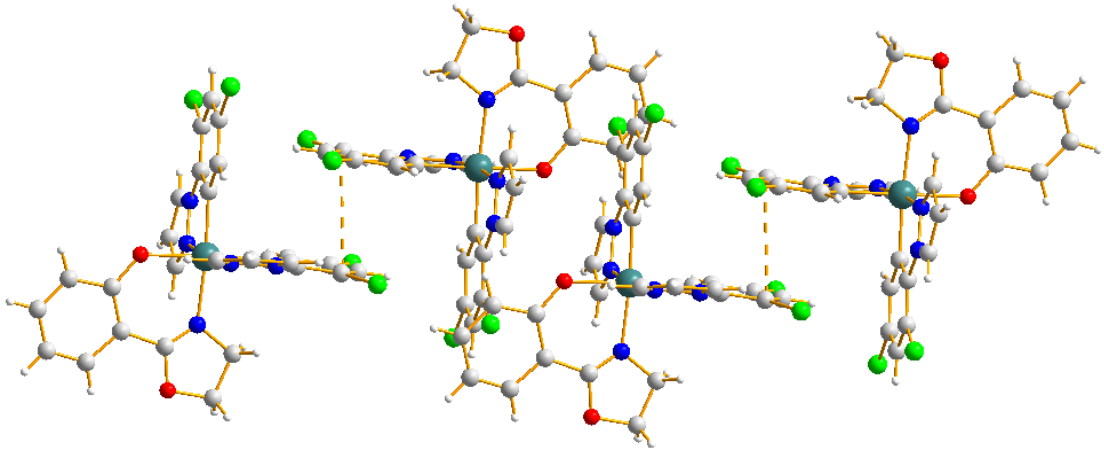

**Fig. S2** Molecular packing of complex **2** in the crystal.

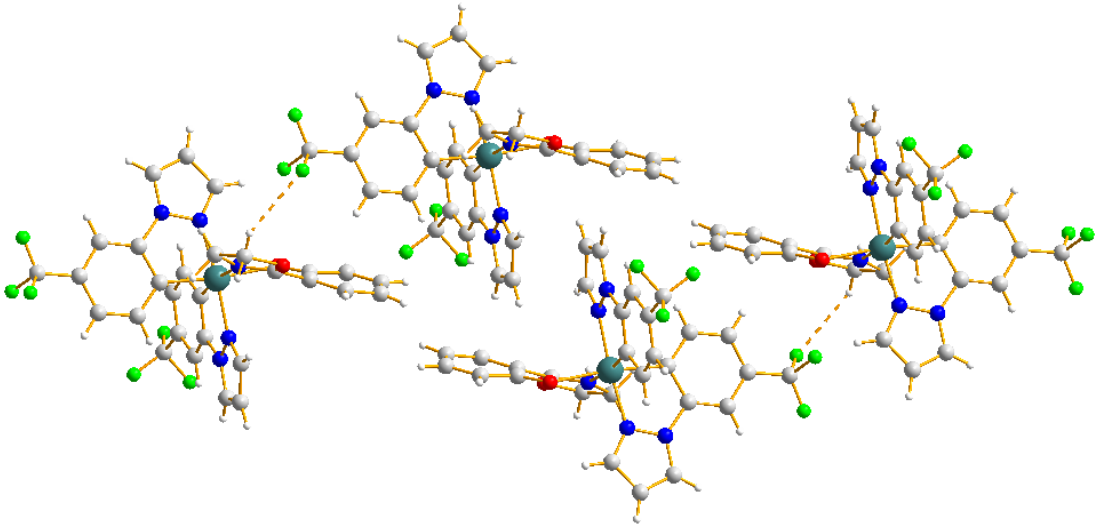

**Fig. S3** Molecular packing of complex **3** in the crystal.

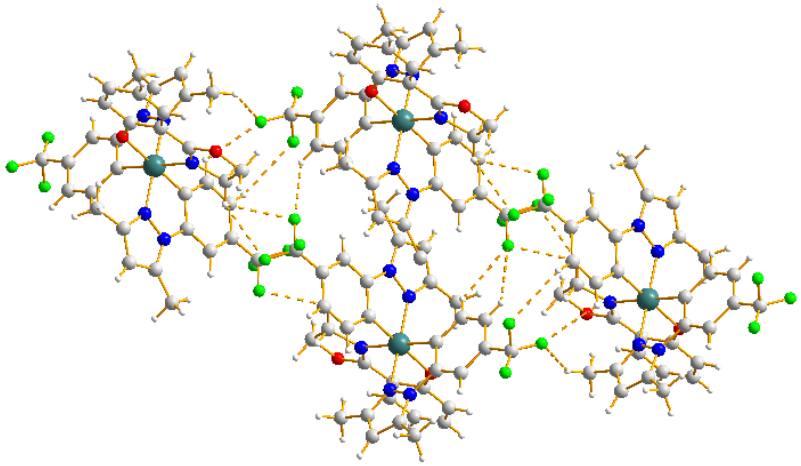

**Fig. S4** Molecular packing of complex **4** in the crystal.

## 4. Photophysical properties

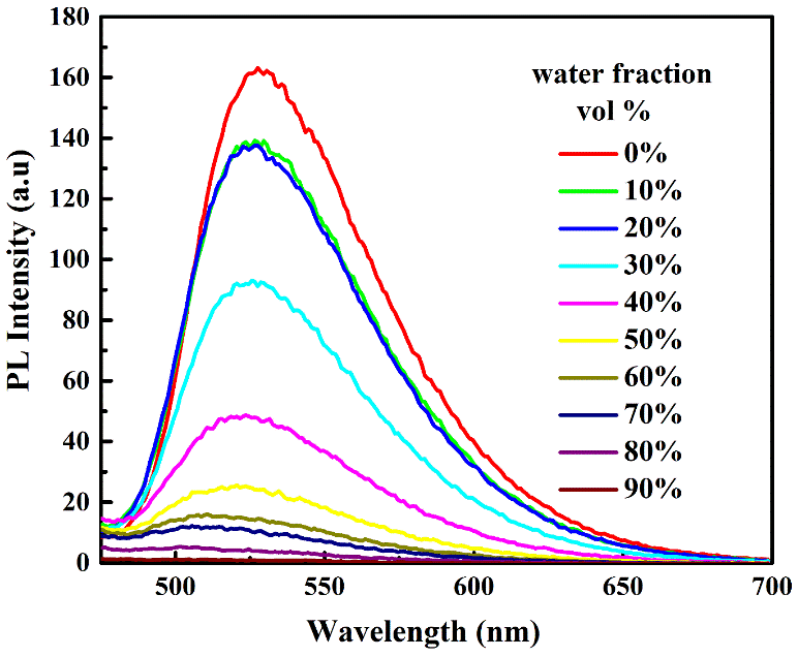


**Fig. S5** The PL spectra of $(ppy)_2Ir(oz)$ (10 μM) in acetonitrile-water mixtures with different water fractions at room temperature.

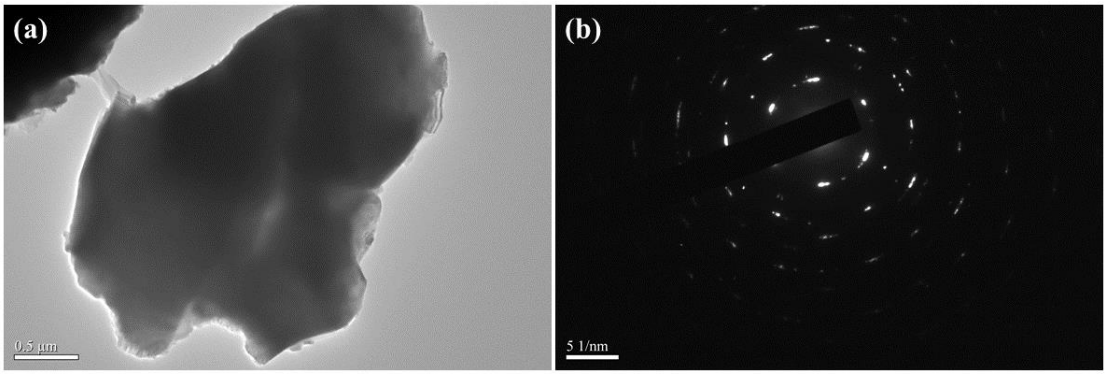


**Fig. S6** (a) TEM image of nanoaggregates of complex **1** formed in acetonitrile-water mixtures with 90% water fraction. (b) The electron diffraction pattern of the nanoaggregates.

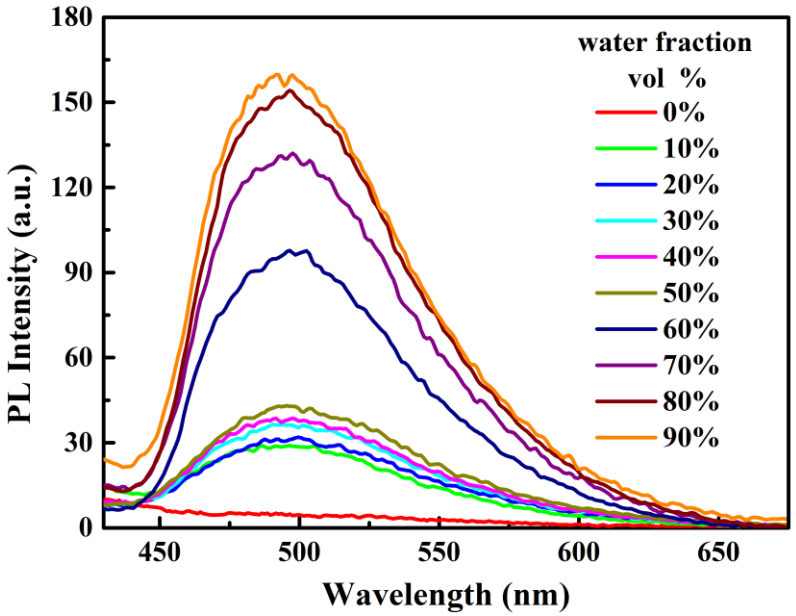


**Fig. S7** PL spectra of complex **2** (10 μM) in acetonitrile-water mixtures with different water fractions at room temperature.

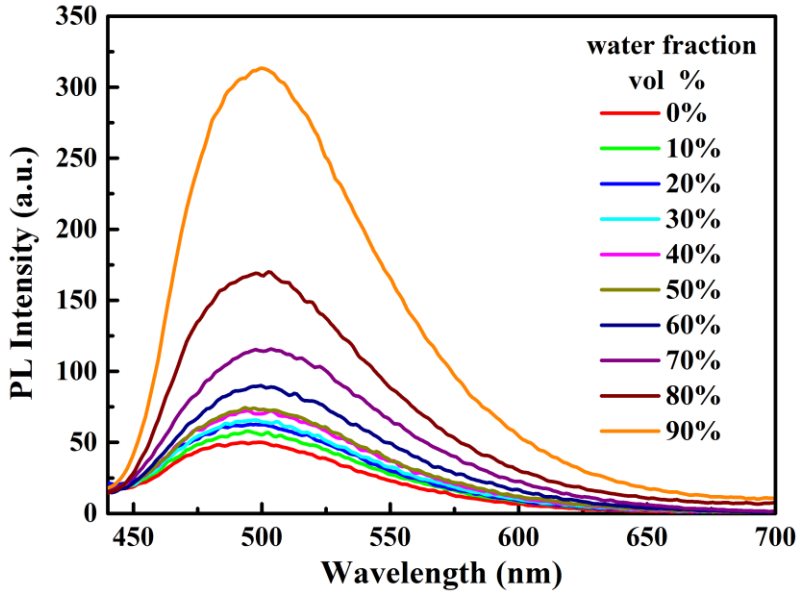


**Fig. S8** PL spectra of complex **3** (10 μM) in acetonitrile-water mixtures with different water fractions at room temperature.

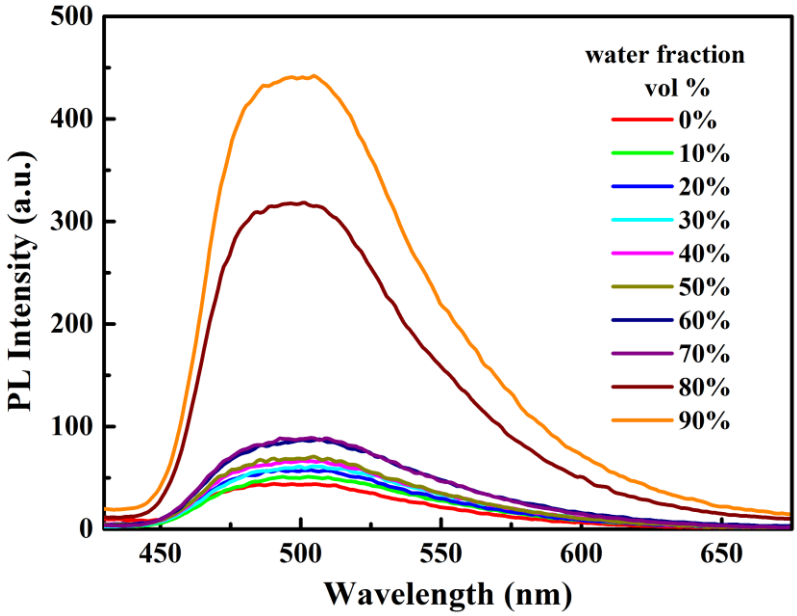


**Fig. S9** PL spectra of complex **4** (10 μM) in acetonitrile-water mixtures with different water fractions at room temperature.

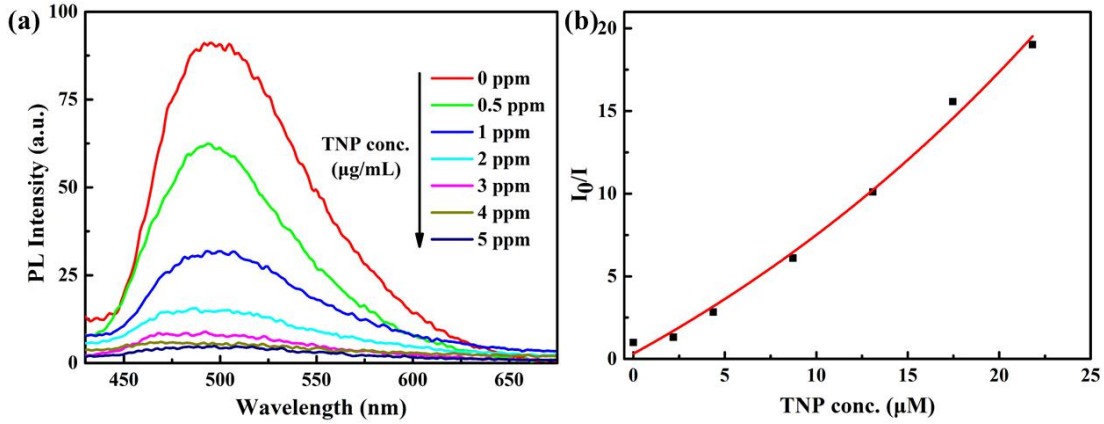


**Fig. S10** (a) PL spectra of complex **2** (10 μM) in acetonitrile-water (v/v = 1:9) containing different amounts of TNP. (b) Corresponding Stern-Volmer plot of TNP.

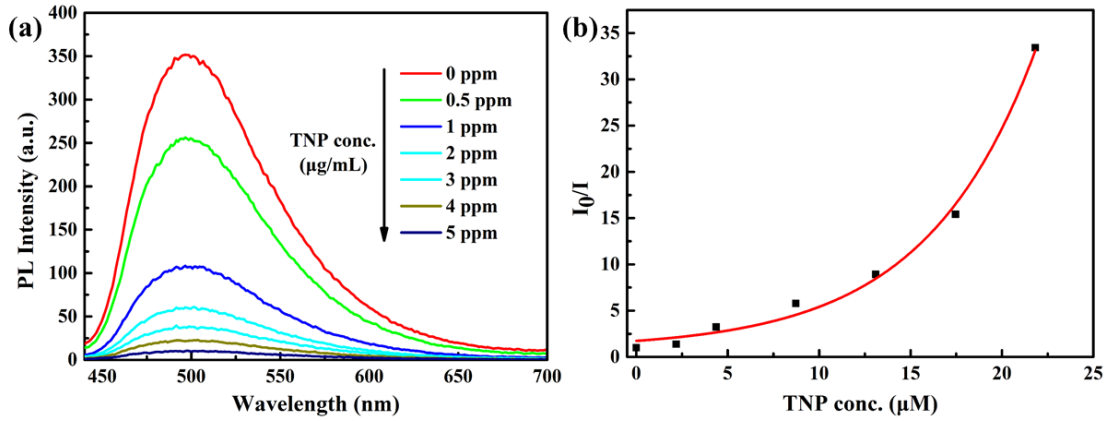


**Fig. S11** (a) PL spectra of complex **3** (10 μM) in acetonitrile-water (v/v = 1:9) containing different amounts of TNP. (b) Corresponding Stern-Volmer plot of TNP.

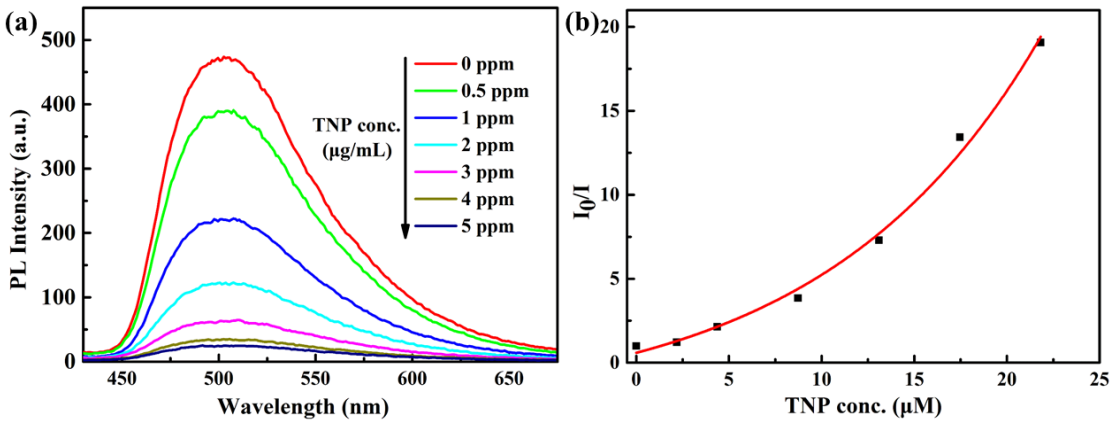


**Fig. S12** (a) PL spectra of complex **4** (10 μM) in acetonitrile-water (v/v = 1:9) containing different amounts of TNP. (b) Corresponding Stern-Volmer plot of TNP.

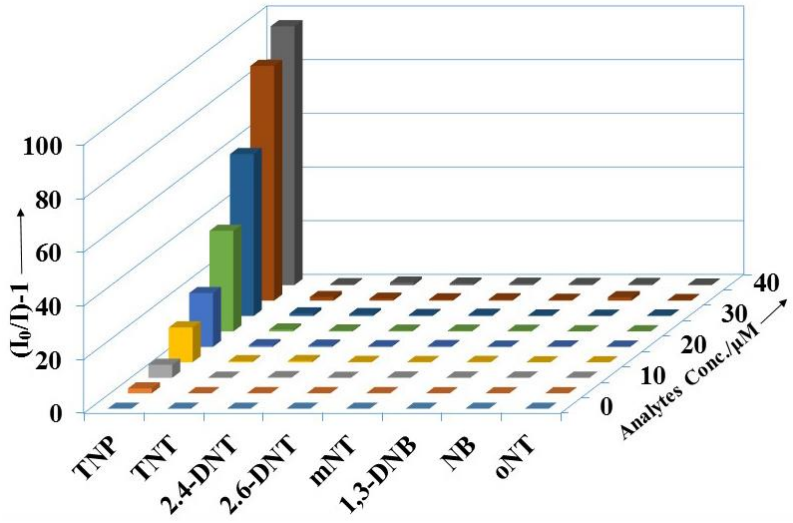


**Fig. S13** Stern-Volmer plot of the emission of complex **1** (10 μM) in the presence of different nitro-atomatic compounds in acetonitrile-water (v/v = 1:9) mixtures.

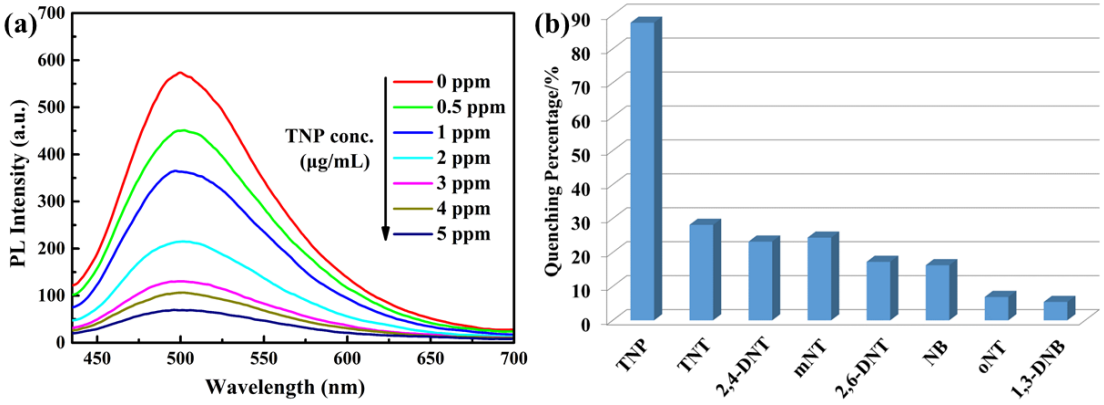


**Fig. S14** (a) PL spectra of complex **1** (10 μM) in $CH_3CN$/aqueous HEPES buffer (1 mM, pH 7.3; 1:4, v/v) solution containing different amounts of TNP. (b) Quenching percentage obtained for different analytes (5 ppm).

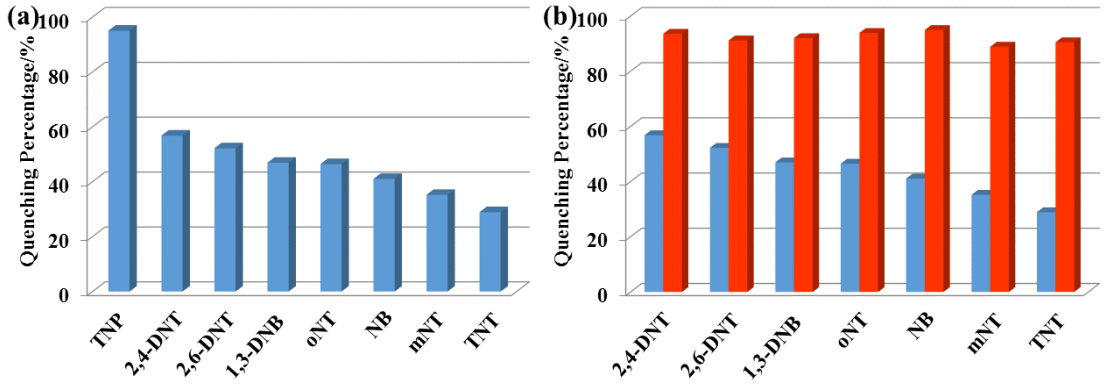


**Fig. S15** (a) Quenching percentage obtained for different analytes (5 ppm). (b) Quenching percentage of complex **2** (10 μM) with analytes (5 ppm) in acetonitrile-water (v/v = 1:9) mixtures before (blue) and after (red) the addition of 5 ppm TNP.

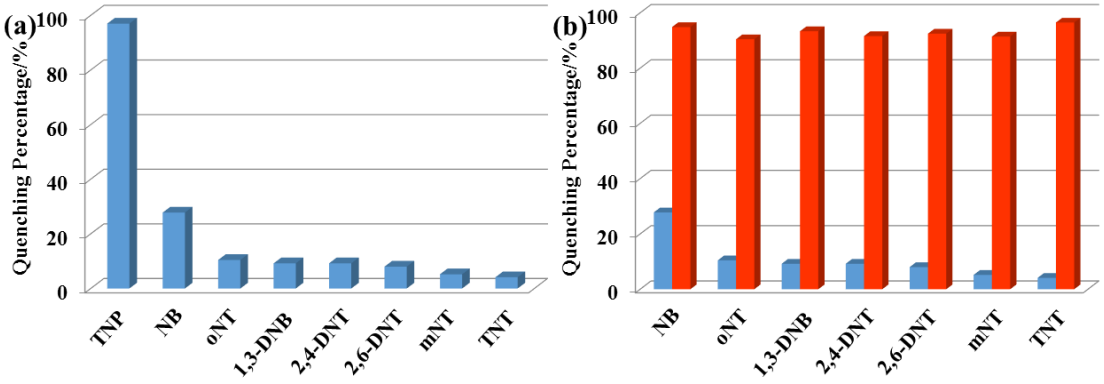


**Fig. S16** (a) Quenching percentage obtained for different analytes (5 ppm). (b) Quenching percentage of complex **3** (10 μM) with analytes (5 ppm) in acetonitrile-water (v/v = 1:9) mixtures before (blue) and after (red) the addition of 5 ppm TNP.

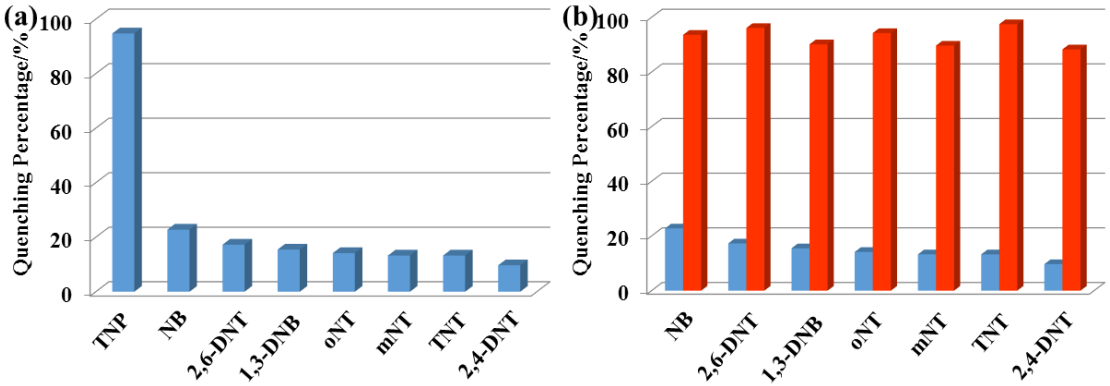


**Fig. S17** (a) Quenching percentage obtained for different analytes (5 ppm). (b) Quenching percentage of complex **4** (10 μM) with analytes (5 ppm) in acetonitrile-water (v/v = 1:9) mixtures before (blue) and after (red) the addition of 5 ppm TNP.

**Structure-property relationships**. The quenching constant of complex **1** is larger than that of complex **2**. The structural difference between complex **1** and complex **2** is the different substituents on the cyclometalated ligands. The more electronegative fluorine atoms in complex **1** can enhance the stability of the Ir-C bond between the cyclometalated ligands and

the metal ion[3] and decrease the stability of the Ir-N (and/or Ir-O) bond between the ancillary ligands and the metal ion according to the *trans* effect.[4] Thus, TNP interacts more easily with the ancillary ligand of complex **1**, resulting in a higher quenching constant. Due to the octahedral structure of this series of complexes, the introduction of methyl groups may increase the steric hindrance and weaken the interaction of O-H···O between TNP and the ancillary ligand of complex **4** compared to **3**, resulting in the smaller quenching constant of complex **4** than that of complex **3**.

## 5. Mechanistic study

TNP can donate a proton to the ancillary ligand leading to decomplexation of the Hoz unit, as shown for complex **1** in Scheme 1. In support of this mechanism, the mass spectrum shows that complex **1** fragments in solution after the addition of TNP (Fig. S18). The mass spectrum of complex **1** (Fig. S18a) has peaks at m/z 714, 736 and 551 which correspond to [complex **1**+H]$^+$, [complex **1**+Na]$^+$ and the (1-(2,4-difluorophenyl)-1*H*-pyrazole)$_2$Ir$^+$ cation. The peaks at m/z 714 and 736 disappear when TNP is added to the solution and the peak at m/z 551 is retained (Fig. S18b). A new peak corresponding to [Hoz+H]$^+$ at m/z 164 appears, which indicates that the Hoz ligand is liberated. $^1$H NMR experiments in DMSO-d$_6$ provide complementary information (Fig. S19). Owing to the octahedral structure of complex **1**, the chemical environment of each of the methylene protons ($H_a$ and $H_b$, $H_c$ and $H_d$) and two pyrazole protons ($H_e$ and $H_f$) are different. When complex **1** is mixed with TNP, the protons show an obvious change of chemical shift. $H_a$ and $H_b$, $H_c$ and $H_d$, $H_e$ and $H_f$ combine into three peaks, each representing two hydrogens, indicating that their chemical environments become the same. These data suggest that the octahedral structure of complex **1** is disrupted by the addition of TNP. $^{19}$F NMR analysis of the mixture of complex **1** and TNP further supports these data (Fig. S20). 1-iodo-3-(trifluoromethyl)benzene was added as an internal standard. The four different chemical environments for the fluorine atoms in the octahedral structure of complex **1**, give rise to four peaks in the $^{19}$F NMR spectrum. The addition of TNP leads to only two peaks in the $^{19}$F NMR spectrum due to two different of chemical environments of the fluorine atoms. These results are entirely consistent with the mechanism in Scheme 1. The mechanism of TNP detection by complexes **2-4** is the same as for complex **1** (Fig. S21-S26).

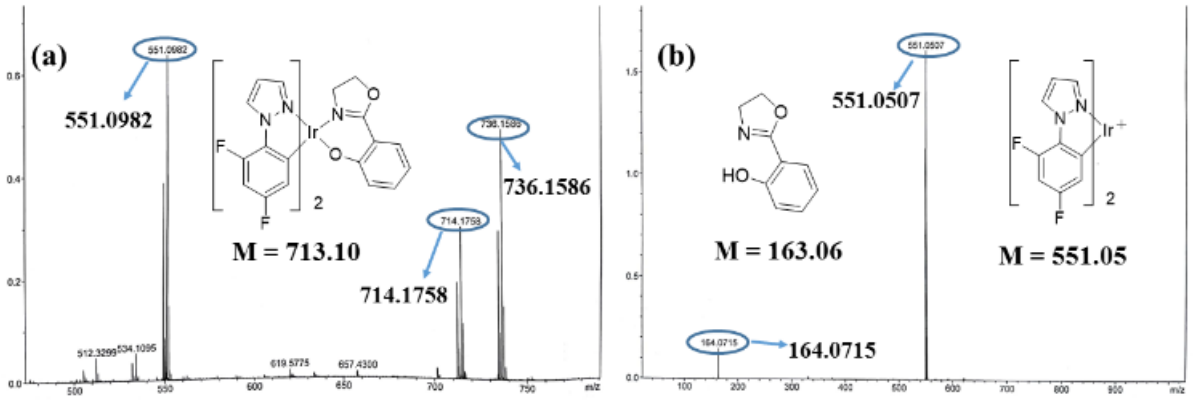


**Fig. S18** Mass spectrum of complex **1** (a) before and (b) after addition of 1 equivalent of TNP.

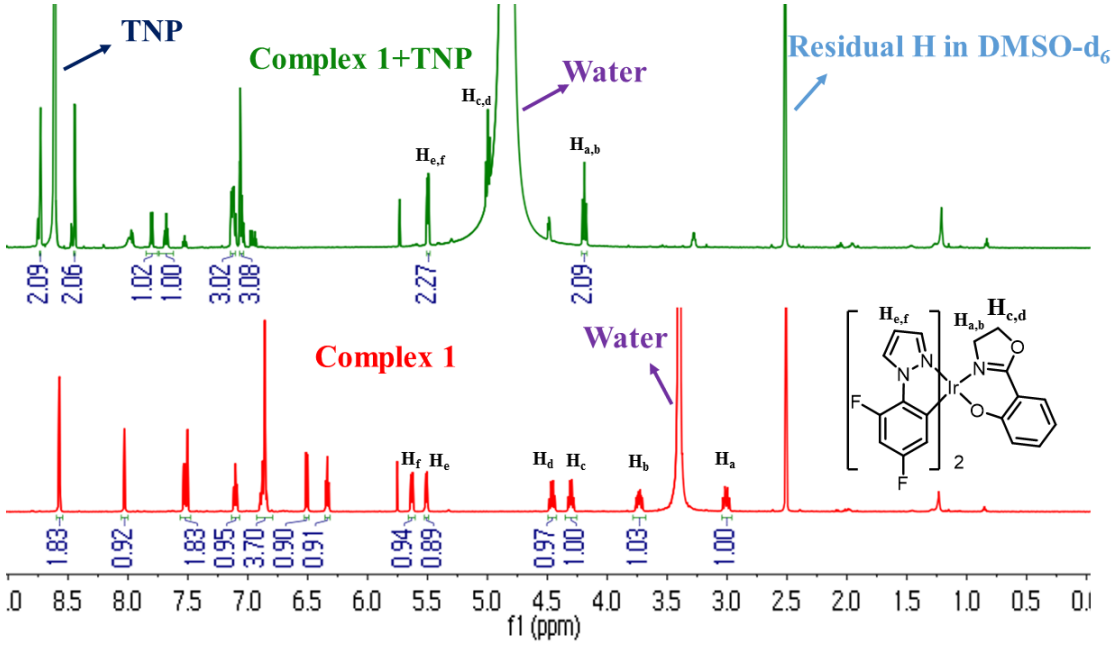


**Fig. S19** $^{1}$H NMR spectra of complex **1** before and after addition of 1 equivalent of TNP in DMSO-$d_6$.

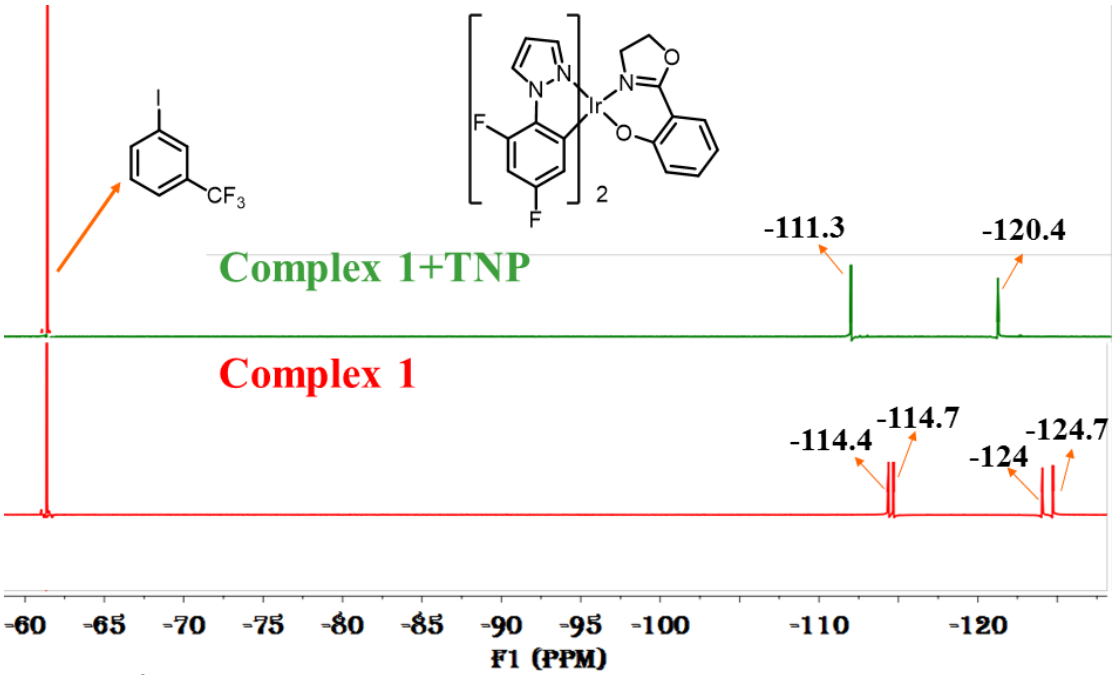


**Fig. S20** $^{19}$F NMR spectra of complex **1** before and after addition of 1 equivalent of TNP in DMSO-$d_6$ (internal standard = 1-iodo-3-(trifluoromethyl)benzene).

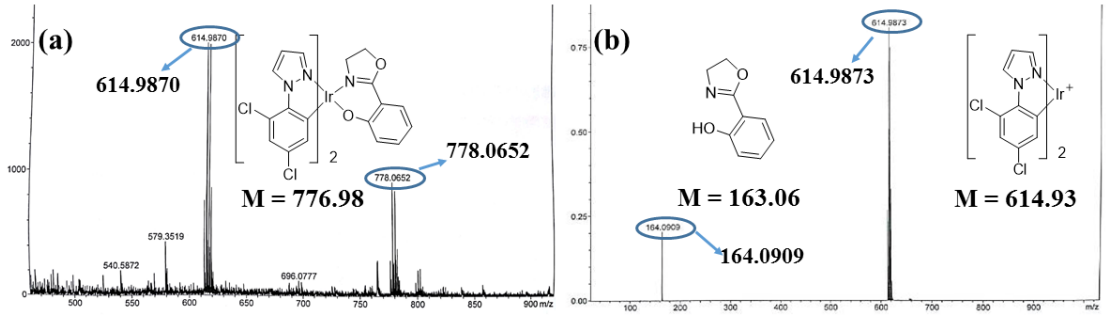


**Fig. S21** Mass spectrum of complex **2** (a) before and (b) after addition of 1 equivalent of TNP.

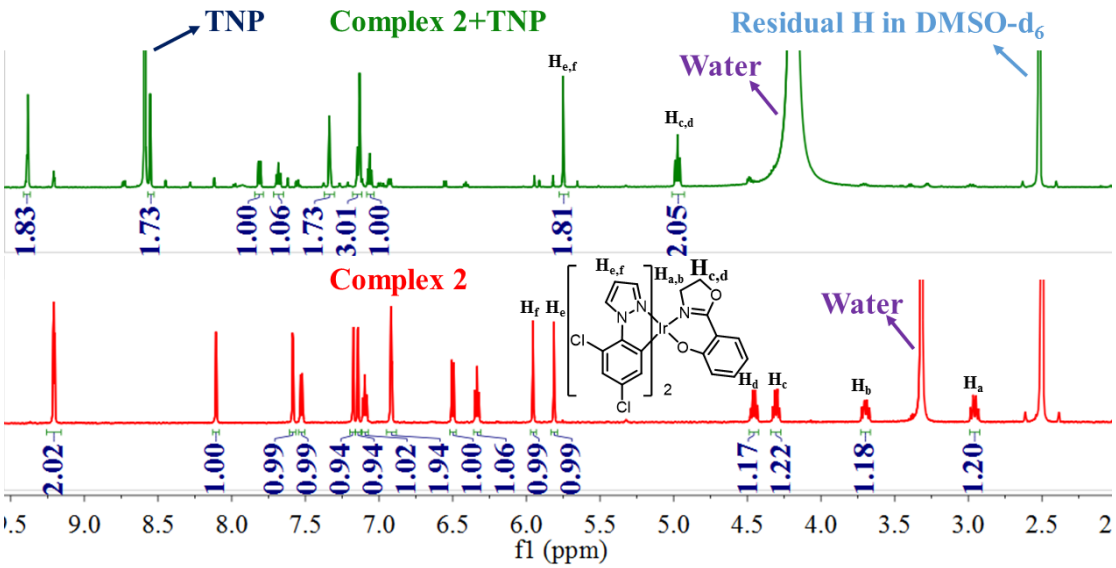


**Fig. S22** $^{1}$H NMR spectra of complex **2** before and after addition of 1 equivalent of TNP in DMSO-$d_6$. The $H_a$ and $H_b$ in complex **2**+TNP are contained in the peak of water.

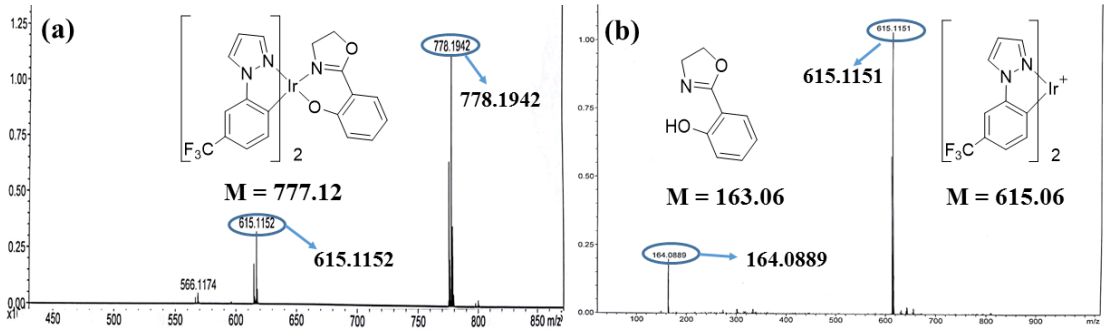


**Fig. S23** Mass spectrum of complex **3** (a) before and (b) after addition of 1 equivalent of TNP.

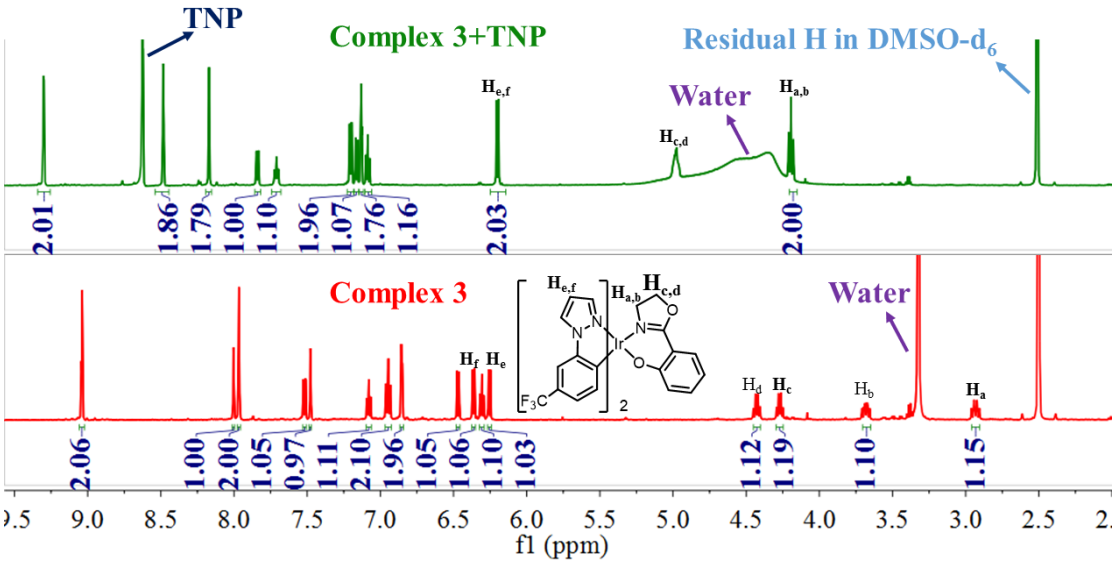


**Fig. S24** $^{1}$H NMR spectra of complex **3** before and after addition of 1 equivalent of TNP in DMSO-$d_6$.

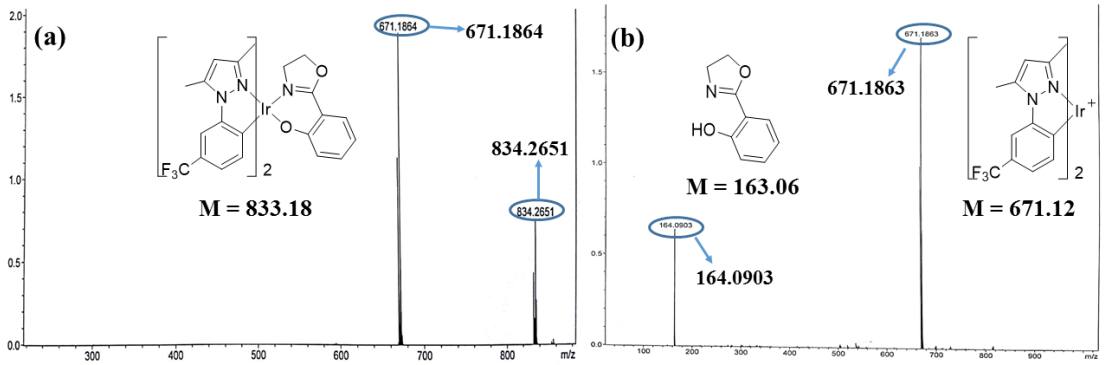


**Fig. S25** Mass spectrum of complex **4** (a) before and (b) after addition of 1 equivalent of TNP.

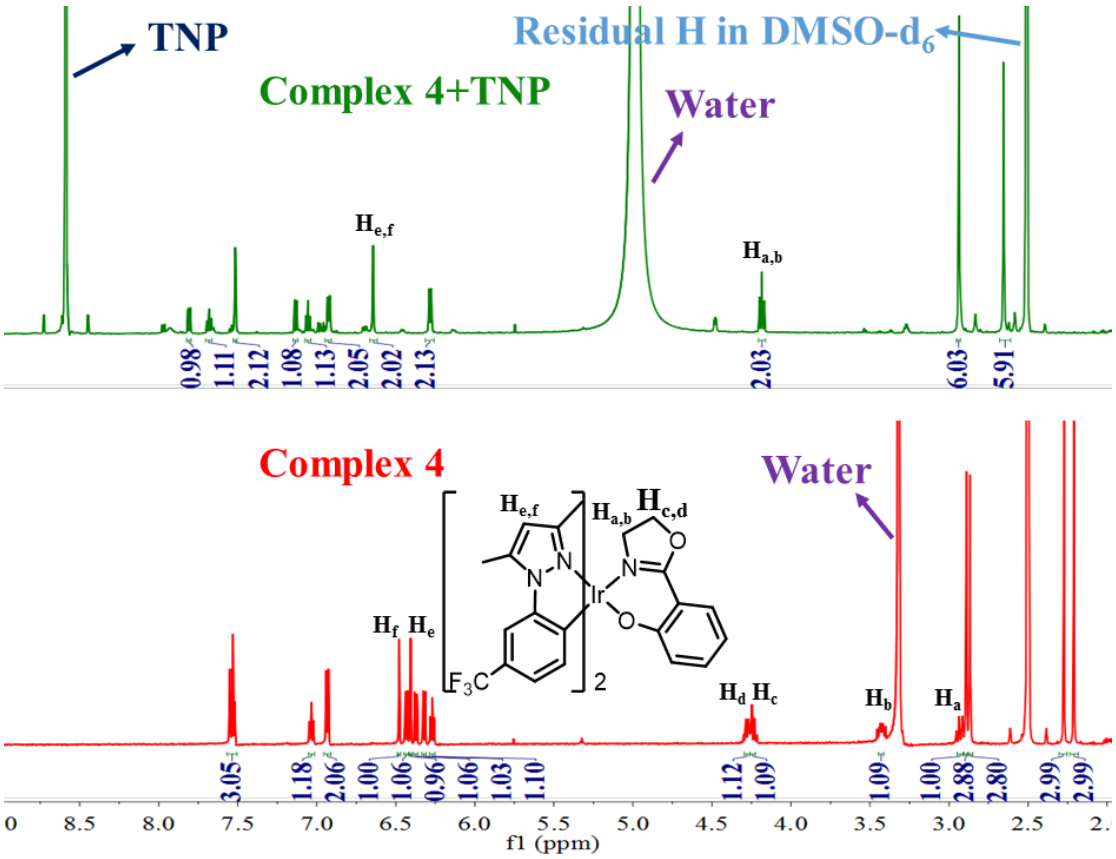


**Fig. S26** $^{1}$H NMR spectra of complex **4** before and after addition of 1 equivalent of TNP in DMSO-$d_6$. The $H_c$ and $H_d$ in complex **4**+TNP are contained in the peak of water.

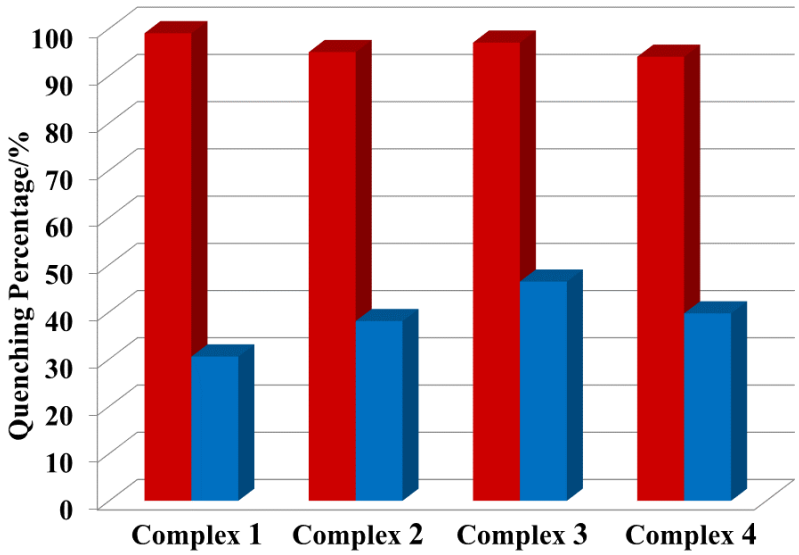


**Fig. S27** Quenching percentage of complexes **1-4** (10 μM) with 5 ppm of TNP (red) and 2,4-DNP (blue) in acetonitrile-water (v/v = 1:9).

## 6. Theoretical calculations

To gain a better understanding of the experimental results, theoretical calculations were performed with Gaussian 09 program.[5] The geometry optimizations were performed by B3LYP methods. The B3LYP functional was employed for all DFT calculations. The 6-31G*

basis set was employed for C, H, N, O, F, Cl atoms, while the iridium atom was described by the Hay-Wadt effective core potential (ECP) and a double-ξ basis set LANL2DZ. The highest occupied molecular orbital (HOMO) and lowest unoccupied molecular orbital (LUMO) energy levels based on the optimized ground-state geometries were calculated (Fig. S27).

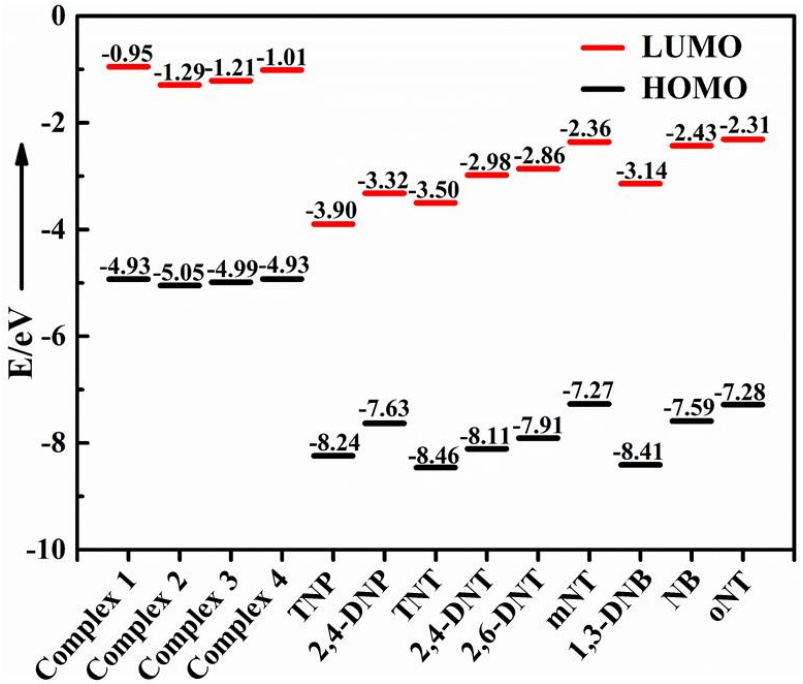


**Fig. S28** Calculated HOMO and LUMO energies of complexes **1-4** and the nitro-aromatic explosives.

## 7. References


1. W. L. Che, T. C. Yu, D. Jin, X. Y. Ren, D. X. Zhu, Z. M. Su and M. R. Bryce, *Inorg. Chem. Commun.*, 2016, **69**, 89.
2. (a) G. G. Shan, H. B. Li, Z. C. Mu, D. X. Zhu, Z. M. Su and Y. Liao, *J. Organomet. Chem.*, 2012, **702**, 27; (b) E. Baranoff, H. J. Bolink, E. C. Constable, M. Delgado, D. Häussinger, C. E. Housecroft, M. K. Nazeeruddin, M. Neuburger, E. Ortí, G. E. Schneider, D. Tordera, R. M. Walliser and J. A. Zampese, *Dalton Trans.*, 2013, **42**, 1073.
3. J. A. Garg, O. Blacque, T. Fox and K. Venkatesan, *Inorg. Chem.*, 2010, **49**, 11463.
4. J. V. Quagliano and L. Schubert, *Chem. Rev.*, 1952, **50**, 201.
5. M. J. Frisch, G. W. Trucks, H. B. Schlegel, G. E. Scuseria, M. A. Robb, J. R. Cheeseman, G. Scalmani, V. Barone, B. Mennucci, G. A. Petersson, H. Nakatsuji, M. Caricato, X. Li, H. P. Hratchian, A. F. Izmaylov, J. Bloino, G. Zheng, J. L. Sonnenberg, M. Hada, M. Ehara, K. Toyota, R. Fukuda, J. Hasegawa, M. Ishida, T. Nakajima, Y. Honda, O. Kitao, H. Nakai, T. Vreven, J. A. Montgomery, Jr., J. E. Peralta, F. Ogliaro, M. Bearpark, J. J. Heyd, E. Brothers, K. N. Kudin, V. N. Staroverov, R. Kobayashi, J. Normand, K. Raghavachari, A. Rendell, J. C. Burant, S. S. Iyengar, J. Tomasi, M. Cossi, N. Rega, J. M. M. Millam, M. Klene, J. E. K. Knox, J. B. C. Cross, V. Bakken, C. Adamo, J. Jaramillo, R. Gomperts, R. E. Stratmann, O. Yazyev, A. J. Austin, R. Cammi, C. Pomelli, J. W. Ochterski, R. L. Martin, K. Morokuma, V. G. Zakrzewski, G. A. Voth, P. Salvador, J. J. Dannenberg, S. Dapprich, A. D. Daniels, O. Farkas, J. B. Foresman, J. V. Ortiz, J. Cioslowski and D. J. Fox, Gaussian 09, Revision A.02, Gaussian, Inc, Wallingford CT, 2009.